

Brønsted Acid Organocatalyzed Three-Component Hydroamidation Reactions of Vinyl Ethers

Ivor Smajlagic, Brenden Carlson, and Travis Dudding*

Cite This: *J. Org. Chem.* 2021, 86, 4171–4181

Read Online

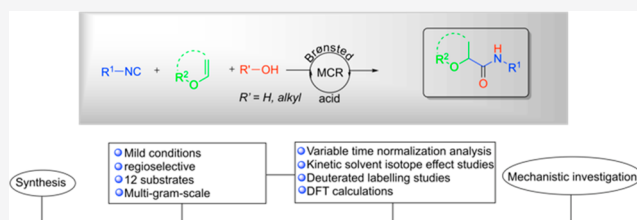
ACCESS |

Metrics & More

Article Recommendations

Supporting Information

ABSTRACT: Hydroamidation of carbon–carbon double bonds is an attractive strategy for installing nitrogen functionality into molecular scaffolds and, with it, increasing molecular complexity. To date, metal-based approaches have dominated this area of chemical synthesis, despite the drawbacks of air and moisture sensitivity, limited functional group tolerance, toxicity, and/or high cost often associated with using metals. Here, in offering an alternative solution, we disclose an operationally simple, metal-free, one-pot, regioselective, multicomponent synthetic procedure for the hydroamidation of carbon–carbon double bonds. This method features mild reaction conditions and utilizes isocyanides and vinyl ethers for the rapid and modular synthesis of privileged α -oxygenated amide scaffolds. In unraveling the mechanistic underpinning of this non-metal-based reactivity, we present kinetic solvent isotope effect studies, variable time normalization analysis, and density functional theory computations offering insight into the mechanism of this multistep catalytic hydroamidation process.



INTRODUCTION

The selective introduction of amide functionality into organic molecules is of the utmost importance, and transformations for achieving this goal are of fundamental interest in organic synthesis and paramount to the chemical and life science industries.^{1,2} This significance spans from the manifold roles of amides in Nature, where they are the centerpiece of proteins, e.g., enzymes, in essence the fabric and working machinery of living systems. With this, amides are found in numerous drug scaffolds and biologically active compounds, including natural products, heterocycles, polymers, and pharmaceutical drugs, with nearly two-thirds of drug candidates containing this privileged functionality.³ Notwithstanding, the efficient and selective introduction of amides⁴ into organic molecules under mild catalytic conditions that are tolerant of various functional groups is a formidable challenge with practical limitations. Traditional synthetic strategies toward amide formation rely upon the condensation of carboxylic acids and their derivatives with amines in the presence of stoichiometric amounts of activating or coupling reagents. While tried and true, these methods are at a disadvantage because of the use of toxic, hazardous, and/or costly coupling reagents generating equivalents of waste, thus complicating product isolation and driving up costs.⁵ For instance, benzotriazole-based aminium salts, such as HATU,⁶ HCTU,⁷ and HBTU,⁸ are considered as class 1 explosives, showing autocatalytic decomposition, difficult handling during transport and storage,⁹ and their use results in stoichiometric equivalents of byproduct waste.

Though viable, the use of coupling reagents for amide formation is subpar in terms of meeting the goal of global

sustainability enabling productive harmony, stability, and resilience to support present and future generations. To bypass these drawbacks, catalytic methods for the formation of amides and their selective installation into organic molecules have attracted considerable attention. These methods include oxidative amidation using amine precursors,¹⁰ hydrocarbonylation of alkenes/alkynes,¹¹ oxidative coupling of α -bromo nitroalkanes with amines,¹² transamidation reactions,¹³ and acylation of amines.¹⁴ These catalytic procedures, however, are not free of limitations, as many are restricted by the use of costly, toxic metals and harsh reaction conditions requiring excessive heating and long reaction times.^{4,15} Moreover, the metals used in the procedures may engage in nonspecific coordination with synthesized amide bonds.^{11h} A particularly productive alternative, however, has been the use of either boron-based catalysts or group(IV) metals to catalytically induce direct amidation.¹⁶ Nonetheless, more environmentally benign methods implementing organocatalytic conditions for amide formation—ideally using low catalyst loadings—are highly desirable.

By the same token, the advancement of novel modes of catalysis enabling access to amides or, more broadly, less

Received: December 23, 2020

Published: February 24, 2021



explored or uncharted modes of bond construction is a powerful way of increasing chemical space. On this front, the use of isocyanides as linchpins for innovative modes of bond formation has witnessed a renaissance over the past two decades, owing to their rich, diverse, and ambiphilic reactivity profiles.^{17,18} Isocyanide-based multicomponent reactions (IMCRs),¹⁸ as one of the most efficient and operationally simple methods, attest to this fact. This is clearly seen from their use in diversity-oriented synthesis (DOS) and construction of valuable molecules, such as heterocyclic cores in natural products.¹⁹ Moreover, various Passerini,²⁰ Ugi,²¹ and related IMCR transformations are reported, many of which proceed by reaction mechanisms relying upon Lewis acid catalysis or organocatalysis.²² While these achievements are impressive, an overarching feature of these reactivities is the limited use of polar C=X (X = O, N) bonds^{23–26} along with a handful of examples of polar C=C or C≡C bonds as the electrophilic component.^{24e,27}

In view of this current state, coupled with our interest in oxocarbenium functionalization,²⁸ the prospect of developing an organocatalyzed hydroamidation reaction furnishing amide products attracted our attention. As a point of departure for this undertaking targeting unique catalytic reactivity for amide formation, we turned to the blueprint of retrosynthetic analysis to identify viable precursors (synthons) for accessing distinctive bond connectivity. To this end, we arrived at the transformation depicted in Figure 1A tracing back to the

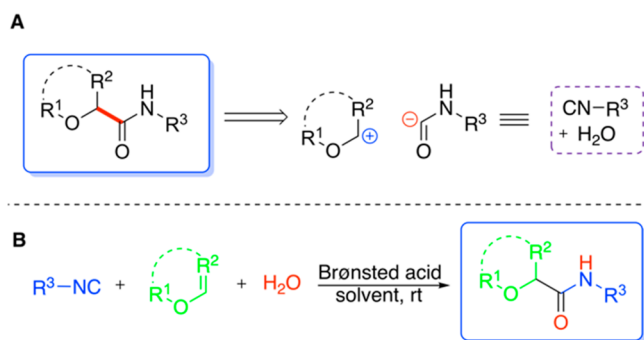


Figure 1. Envisioned approach to access α -oxygenated amides.

disconnection of a carbenium- and amide acyl anion synthons; the former derived from vinyl ether protonation, while the latter arises from isocyanide and H₂O synthetic equivalents. Notably, in the forward direction, this novel mode of catalysis shares hallmarks of IMCR Passerini-type reactivity allowing atom-economical access to synthetically attractive α -oxygenated amides (Figure 1B). Moreover, this posited reactivity would expand the scope of IMCR transformations beyond its heavy reliance upon electrophilic carbonyl and alkene/alkyne components by employing vinyl ethers.

Curious as to the mechanistic features of this putative reactivity, and, with it, the goal of rendering a robust catalytic method, we embarked upon the current study. In this interest, our primary objective was to provide a comprehensive mechanistic study with facets rooted in multicomponent Passerini-type reactivity, ultimately leading to innovative metal-free catalysis for amide formation. Along with this advancement was exploration of the innate preferences of ambiphilic isocyanide reactivity with vinyl ethers. Accordingly, we present herein the successful development of a one-pot, multicomponent, Brønsted acid organocatalyzed hydroamida-

tion reaction of carbon–carbon double bonds providing synthetically relevant amide-containing compounds from isocyanides and vinyl ethers under mild conditions with regioselectivity. Critical to this work were mechanistic studies including variable time normalization analysis (VTNA),²⁹ kinetic solvent isotope effect (KSIE) experiments, and density functional theory (DFT) calculations.

RESULTS AND DISCUSSION

At the outset of this study, the following queries of concern materialized: Can we enable catalytic turnover? What Brønsted acid(s) would be optimal? How might we minimize non-productive byproduct formation, e.g., hydration of vinyl ethers and/or isocyanides? In entertaining these questions, we undertook preliminary studies investigating the reaction of easy-to-handle *p*-toluenesulfonylmethyl isocyanide (**1a**) with ethyl vinyl ether (**2a**) and H₂O in the presence of readily available Brønsted acids under several different experimental conditions (Table 1).

These efforts commenced with a scan of different Brønsted acids as potential catalysts under atmospheric conditions open to air (Table 1, entries 1–7). Evident from this survey of acids was that the use of mild acids, such as boric acid and benzoic acid (BzOH), resulted in unreacted starting materials, whereas highly acidic triflic acid (TfOH) led to extensive decomposition of the isocyanide and vinyl ether reagents,³⁰ ultimately revealing (\pm)-10-camphorsulfonic acid (CSA) as a promising lead. We then added stoichiometric amounts of H₂O to the reaction by syringe pump over the course of 4 h with conversion monitored periodically up to 24 h (entries 8–11). Gratifyingly, the addition of 3 equiv of H₂O was found to be optimal in terms of product formation, whereas larger amounts of H₂O (5 to 20 equiv) negatively impacted the reaction owing to formation of formamide (**4**) and 1-ethoxyethanol (**5a**) byproducts, as confirmed by ¹H NMR analysis. Further, the use of dichloromethane (DCM) or 1,2-dichloroethane (DCE) as solvents resulted in slightly lower conversions to the desired product, making tetrahydrofuran (THF) the solvent of choice (entries 12–14). Next, the catalyst loading was sequentially decreased resulting in significant product formation with Brønsted acid CSA at 4 mol % catalyst loading (entries 15 and 16). It is worth noting that a control reaction employing the optimized conditions in the absence of added H₂O provided minuscule amounts of product formation (entry 17). Lastly, cooling the reaction resulted in a decrease in product formation with a concomitant increase in byproducts (entries 18 and 19).

With a viable set of experimental conditions in hand, we turned to VTNA to probe the mechanistic underpinnings of this reaction. Notably, this approach has seen rampant growth in the recent literature owing to its operational simplicity, reliability, and amenability to metal- and metal-free catalysis.^{29,31} The motivation for these analyses was two-fold: (1) to gain fundamental mechanistic understanding of this novel catalytic hydroamidation reaction, especially with respect to the catalyst, and (2) to identify optimal experimental conditions by pinpointing concentration dependences of each respective reaction component.

Accordingly, the reaction of isocyanide **1a** (limiting reagent) and vinyl ether **2a** model substrates, selected for their synthetic utility³² and unobtrusive reactivity profile (i.e., less side product formation), was monitored by ¹H NMR until ~50% consumption of **1a** was observed. Restricting the analyses to

Table 1. Optimization of Reaction Conditions

entry	catalyst (mol %)	solvent	time (h)	H ₂ O (equiv)	3a conversion ^c (%)
1 ^a	boric acid (30)	THF	24		0
2 ^a	BzOH (30)	THF	24		0
3 ^a	4-chlorophenoxyacetic acid (30)	THF	24		<1 ⁱ
4 ^a	3-nitrophthalic acid (30)	THF	24		7 ⁱ
5 ^a	L-tartaric (30)	THF	24		9 ⁱ
6 ^a	TfOH (30)	THF	24		0
7 ^a	(±)-CSA (30)	THF	24		35 (10)
8 ^b	(±)-CSA (30)	THF	24	1	46 (16)
9 ^b	(±)-CSA (30)	THF	24	3	91 (64) ^f
10 ^b	(±)-CSA (30)	THF	24	5	55 (22) ^f
11 ^b	(±)-CSA (30)	THF	24	20	29 (8) ^f
12 ^c	(±)-CSA (30)	THF	2	3	93 (66) ^f
13 ^c	(±)-CSA (30)	DCM	2	3	85 (59) ^f
14 ^c	(±)-CSA (30)	DCE	2	3	84 (56) ^f
15 ^c	(±)-CSA (10)	THF	3	3	89 (61) ^f
16 ^{c,d}	(±)-CSA (4)	THF	5	2.5	95 (67) ^f
17 ^d	(±)-CSA (4)	THF	5		<3 ⁱ
18 ^{c,d,g}	(±)-CSA (4)	THF	5	2.5	62 (28)
19 ^{c,d,h}	(±)-CSA (4)	THF	5	2.5	32 (11)

^aReaction conditions: isocyanide (**1a**) (1.0 mmol), ethyl vinyl ether (**2a**) (3.0 mmol), and Brønsted acid (30 mol %) in 0.5 mL of THF were stirred for the indicated time. ^bAfter addition of the aforementioned reactants, H₂O was added over the course of 4 h via syringe pump. ^cH₂O (3.0 mmol) was added immediately. ^d1.2 mmol of **1a** was used. ^eConversion involved monitoring the disappearance of the signal at 7.88 ppm for **1a** and appearance of the signals at 7.76 ppm for product **3a** and 8.03 ppm for side product **4**. Signal overlap between the hydroamidated product, e.g., **3a**, and side product **4** was observed at ~7.76 ppm resulting in constructive interference. This was accounted for when determining product conversion, and thus, product conversion was presented in the absence of inconsistencies. Isolated yields are reported in parentheses. ^fFull consumption of isocyanide (**1a**). ^gReaction was performed at 0 °C. ^hReaction was performed at -20 °C. ⁱIsolated yields could not be determined.

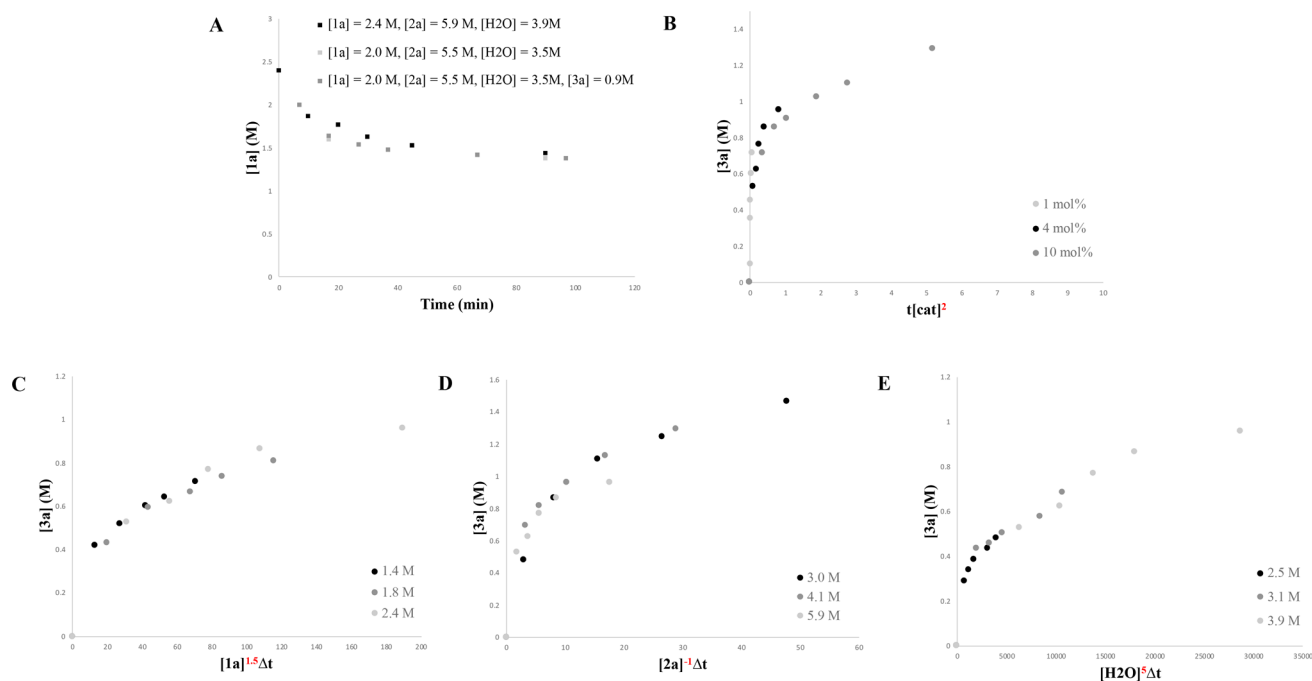


Figure 2. VTNA experimental data with respect to isocyanide consumption for product formation. (A) Plot depicting mild catalyst deactivation. (B) Normalized time scale plot displaying second-order in catalyst. (C–E) Plots revealing concentration dependences on substrates **1a**, **2a**, and H₂O indicating positive 1.5-order, negative first-order, and positive fifth-order, respectively.

this conversion range was required to diminish the effect of inaccuracies arising from potential changes in reaction order. To commence this kinetic investigation, we examined the robustness of the catalyst by reducing the concentrations of

[**1a**]₀, [**2a**]₀, and [H₂O]₀ by 0.4 M, i.e., [**1a**]₀ = 2.4 M, [**2a**]₀ = 5.9 M, and [H₂O]₀ = 3.9 M to [**1a**]₀ = 2.0 M, [**2a**]₀ = 5.5 M, and [H₂O]₀ = 3.5 M. In essence, this experiment allowed for the comparison of the same reaction at different starting

points. In addition, a third experiment was designed to mimic the conditions of experiment 1 (standard conditions) at 45% product conversion. Analysis of the data from these three experiments revealed that product inhibition was an insignificant process and mild catalyst deactivation was occurring instead (Figure 2A). Further, based upon the normalized time scale method^{31b} taking side products into account, the reaction was found to be second-order in catalyst (Figure 2B, see SI for details). From this, two Brønsted acid catalysts in the rate-determining step of the catalytic cycle of this hydroamidation reaction are probable. By analogy, this is in line with the findings from the research groups of Maeda^{20a} and Morokuma^{20c} suggesting two molecules of acid catalyst are involved in the rate-determining step of the Passerini reaction.

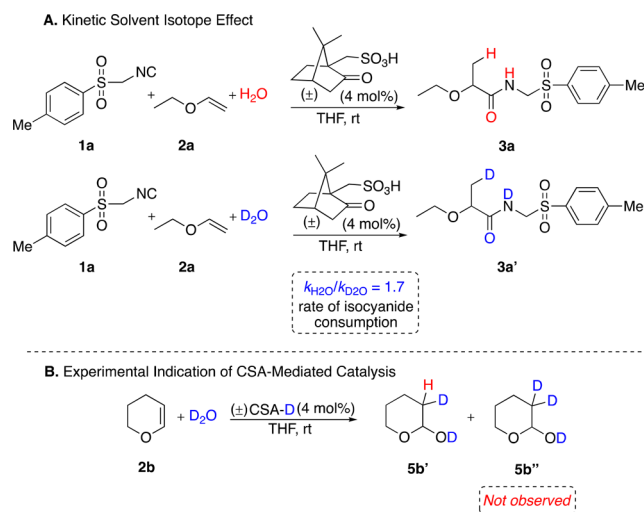
Next, the concentration dependency of each component of this reaction was probed through a series of experiments. This set of experiments was initiated by first delineating the order in isocyanide, which we assigned through visual inspection a positive 1.5-order dependence on [1a] consistent with an accelerated reaction (faster rate) when higher initial substrate concentrations were used (Figure 2C). Conversely, an increase in [2a] led to a decrease in rate consistent with an, arguably, negative first-order dependence in [2a], presumably arising from the formation of a transient acetal involving catalyst CSA and substrate 2a contributing to an unproductive off-cycle equilibrium. Tied to the formation of this acetal was the potential for further reaction with H₂O affording side product 5a (Figure 2D). As a concluding study, we assessed the order in H₂O, which has profound implications toward side product formation. Surfacing from this analysis was a positive order concentration dependence on H₂O, wherein we concluded that a fifth-order assignment was reasonable upon visual inspection (Figure 2e). From these kinetic studies, it is evident that a complex balance of catalyst, isocyanide, vinyl ether and H₂O is required to obtain the desired hydroamidated products.

The generality of these kinetic trends was further probed by additional VTNA studies employing a less reactive vinyl ether, namely 3,4-dihydro-2H-pyran (DHP). Immediately evident from these analyses were more complex reaction profiles with higher populations of side products. Concurrent with these observations were also minor deviations in concentration dependences, though the overall trends remained consistent with the former set of VTNA experiments (see the SI for details).

Our attention then turned to probing the role of nitrilium intermediates in these CSA-catalyzed hydroamidation reactions. In order to gain this insight, a kinetic solvent isotope effect study (Scheme 1A) monitoring relative reaction rates by NMR time-course analysis via tracking isocyanide consumption (1a) in protium or deuterium oxide was performed that resulted in a normal KSIE value ($k_{\text{H}_2\text{O}}/k_{\text{D}_2\text{O}} = 1.7$ at ~50% consumption of 1a). To confine this KSIE value to a sole effect would be questionable as its magnitude encompasses multiple small effects. Irrespective, we ascribe this observed normal KSIE finding to the formation of a transient ion-pair derived from the conjugate base of CSA and a nitrilium species, as KSIE values >1 are anticipated for ion-forming reactions.³³

Finally, to confirm the role of the active catalyst in this reaction, namely Brønsted acid CSA, as opposed to hydronium ion, a simplified system encompassing DHP, D₂O and deuterated CSA was investigated (Scheme 1B). From this experiment, we hoped to distinguish between these two

Scheme 1. Deuterated Labeling Studies



differing modes of catalysis through inspection of the hydrated side product. In theory, the latter would consist of both 5b' and 5b'' as a result of rapid reversible deuteration involving the formation of an ion-pair intermediate from the reactants (specific acid catalysis); see the SI for details. From this study, compound 5b'' was not observed, thus supporting the role of CSA as the active catalyst in mediating proton transfer.

Armed with this mechanistic insight, a tentative catalytic cycle for the hydroamidation of 2a surfaced, wherein three competing pathways presumably exist (Figure 3). One of these was protonation of isocyanide by CSA with subsequent trapping of nitrilium ion by sulfonate. Following this event, formamide production concomitant with catalyst regeneration is realized upon nucleophilic addition of H₂O. Alternatively, CSA-mediated protonation of ethyl vinyl ether provides a CSA–vinyl ether adduct that may further undergo hydration to furnish undesired side product 5a. This is a particularly favorable process at high concentrations resulting in an off-cycle unproductive equilibrium. In order to circumvent this event, a lower concentration of vinyl ether is required from which then two molecules of CSA interact, hence giving rise to the second-order behavior in catalyst. The emerging hydrogen bond (H-bond) catalyst network primes ethyl vinyl ether for rate-limiting isocyanide addition, wherein the nitrilium is trapped by the sulfonate. Finally, a joint effort between CSA and H₂O transpires with the latter serving a two-part function, including generating the desired α -oxygenated amide product and turning over the catalyst.

From this putative mechanistic interpretation, we turned to DFT calculations at the ((IEFPCM)_(THF))B3LYP/6-311++G(2d,p)//B3LYP/6-31+G(d,p) level using the Gaussian 09 program³⁴ to gain further insight and corroborate our working proposal for hydroamidation. In this effort, methanesulfonic acid was used in place of CSA, while the remaining reaction components included *tert*-butyl isocyanide and ethyl vinyl ether. From these computational studies emerged the pathway depicted in Figure 4. At the outset of the pathway, intermediate IM1 reacts by concerted proton transfer transition state (TS1) with C···H and C···O bond-forming distances of 1.27 Å and 2.64 Å and a low Gibbs free energy activation barrier (ΔG^\ddagger) of 10.3 kcal mol⁻¹. As a finer detail, it is notable the concerted nature of TS1 contrasts with stepwise proton transfer, as suggested in the catalytic cycle of Figure 3.

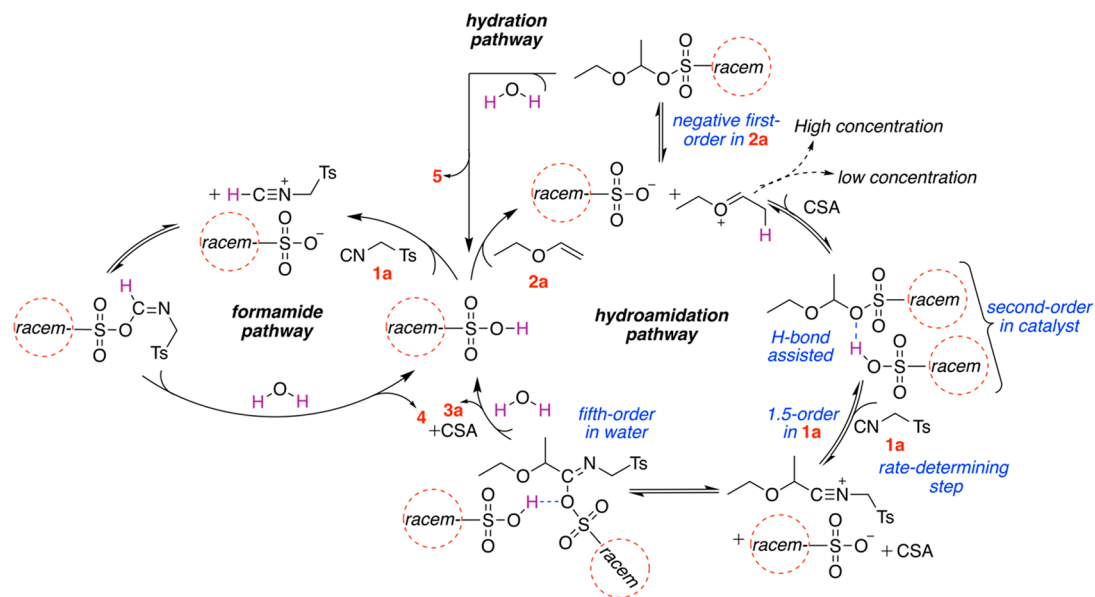


Figure 3. Tentative catalytic cycle based on experimental kinetic studies.

Next, in the presence of another molecule of catalyst and isocyanide, intermediate **IM3**, via a tricomponent complex, reacts by S_N2 -like transition state³⁵ (**TS2**) with an activation barrier of 19.5 kcal mol⁻¹ to provide intermediate **IM4**. The key features of this transition state includes a C...C bond-making distance of 2.17 Å and a C...O bond-breaking distance of 3.27 Å. Overall, this endergonic process involving two molecules of catalyst is the rate-limiting step, thus corroborating our initial conjecture. What is more, the 5.2 kcal mol⁻¹ difference in stability between intermediates **IM2** and **IM4** is consistent with an irreversible process having a negative first-order concentration dependence on the vinyl ether component. Further, these computed results involving the intermediacy of charged nitrilium species **IM4** is in line with our KSIE findings.

At this juncture, we rule out nitrilium trapping with another equivalent of catalyst owing to transition state **TS3_C** (C = catalyst addition) ($\Delta G^\ddagger = 13.3$ kcal mol⁻¹) being more energetically demanding. The product of this transition state (intermediate **IM5**) is 14.3 kcal mol⁻¹ less stable than intermediate **IM1** (blue line), and, thus, this pathway was not further investigated. Alternatively, more feasible was trapping of the incipient nitrilium species with H₂O operating through a concerted process. The activation barrier for this event was found to be marginally lower ($\Delta G^\ddagger = 12.3$ kcal mol⁻¹), relative to intermediate **IM4**, formed from transition state **TS3_H** (H = H₂O) featuring C...O and O...H bond forming distances of 1.94 Å and 1.60 Å, respectively. A distinct feature of this transition state was a unique 10-membered H-bond network priming H₂O for nucleophilic addition and concomitant proton transfer yielding **IM7** residing 10.7 kcal mol⁻¹ below intermediate **IM5** on the reaction coordinate. Tautomerization of **IM7** then furnishes product **3'**, presumably by a simple stepwise acid–base mechanism.³⁶ The specific details of this transformation were not further investigated as tautomerization processes are a contentious subject inevitably marred in ambiguity and, for that matter, not readily tractable in computational investigations.

Having a firm understanding of the mechanism at hand, the substrate scope of hydroamidation of vinyl ethers was then

investigated (Figure 5). Various isocyanides (**1a–c**) and endocyclic, exocyclic, and short-chain vinyl ethers (**2a–d**) reacted to furnish hydroamidated products (**3a–3f**) in low-to-good yields (35–71%). Further, additional complex vinyl ether products (**3g–3l**) were obtained using a slightly modified procedure substituting water for alcohol. Long-chain vinyl ethers provided products **3g–i** in moderate yields (40–48%), while more complex and bulky vinyl ether substrates afforded products **3j** and **3k** in low-to-moderate yields (41% and 31%, respectively), displaying the negative impact of sterics upon product formation.

Comparatively, negligible differences in yield were observed for more substituted vinyl ethers (**3l**, 41%). In probing other reaction centers, the methodology was found to be unreactive toward unactivated alkenes and alkynes.³⁷ Moreover, in demonstrating synthetic utility, we performed a multigram-scale reaction that afforded compound **3a** in 62% yield (Scheme 2).

CONCLUSION

In closing, a Brønsted acid organocatalyzed hydroamidation of vinyl ethers using readily available reagents in a one-pot, three-component reaction has been developed. The strengths of this protocol include operational simplicity, environmentally benign reaction conditions, regioselectivity, and fast reaction times. Detailed VTNA studies revealed concentration dependences of reaction components as well as catalyst deactivation. Further, kinetic solvent isotope effect studies supported the presence of a nitrilium ion pair as a key intermediate in this reaction. Corroborating these experimental findings were computations offering insight into the mechanism of this amide-forming reactivity from which isocyanide addition was pinpointed as the rate-limiting step. Collectively, this work provides an innovative strategy for accessing α -oxygenated amide products that complement current metal-based approaches.

EXPERIMENTAL SECTION

Computational Methods. Quantum mechanical calculations were performed using the Gaussian 09 software package.³⁴ All

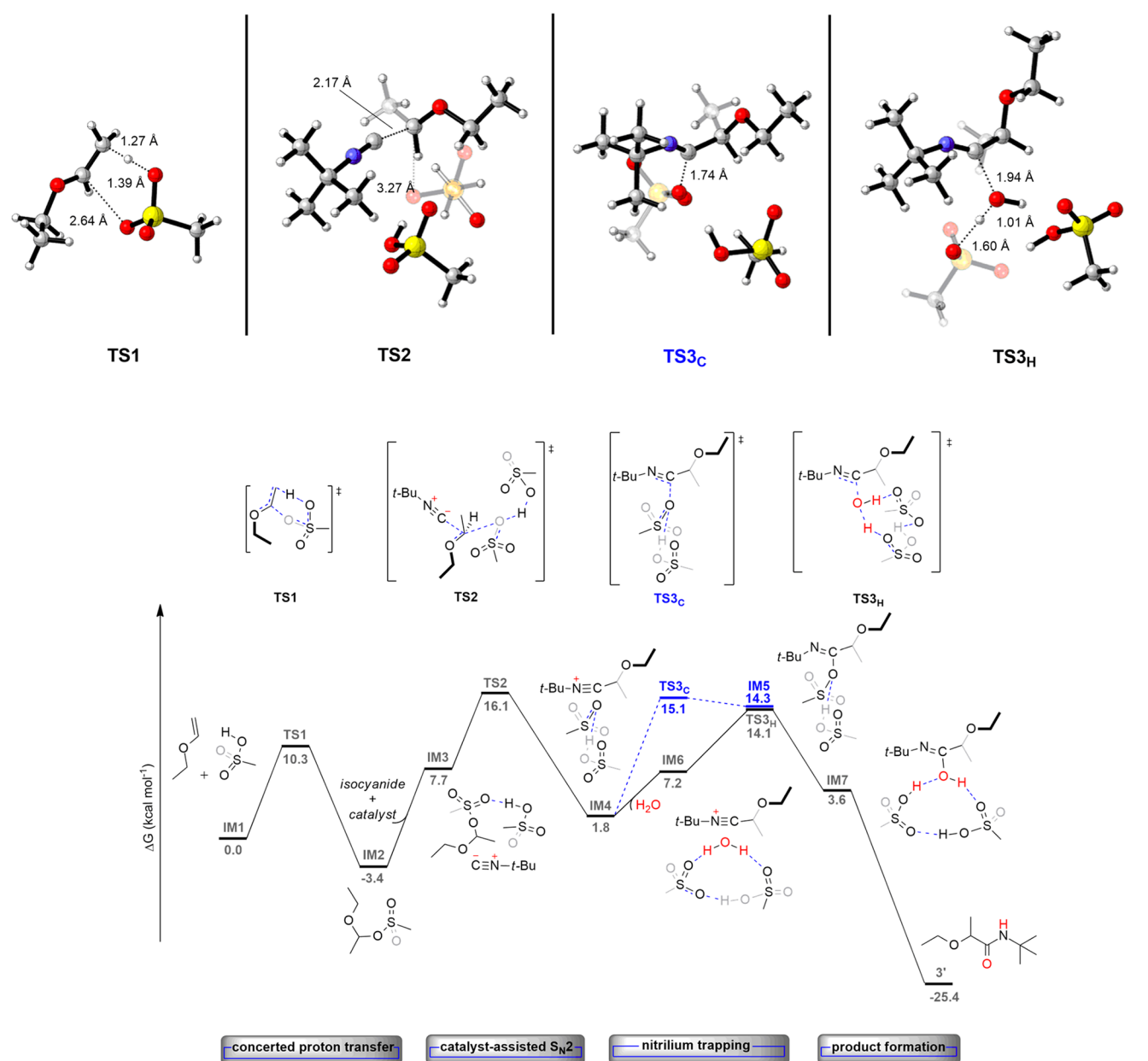


Figure 4. Free energy profile for the CSA-mediated hydroamidation of vinyl ethers.

geometry optimizations were performed using the B3LYP functional³⁸ with a 6-31+G(d,p) basis set. The optimized geometries were verified as transition state structures (one imaginary frequency) or minima (zero imaginary frequencies) by frequency calculations. Intrinsic reaction coordinate (IRC) calculations^{39,40} were performed to confirm that all transition state structures were linked to relevant minima. The energies of the B3LYP/6-31+G(d,p)-optimized structures were further refined by single-point calculations performed at the B3LYP/6-311++G(2d,p) level of theory using the integral equation formalism polarizable continuum model (IEFPCM) with the default parameters of THF ($\epsilon = 7.43$) to account for solvent.⁴¹ The final reported Gibbs free energies are the summed thermal corrections to the Gibbs free energies (temperature = 298.15 K) computed at the lower (B3LYP/6-31+G(d,p)) level of theory and electronic energies from single-point B3LYP/6-311++G(2d,p) calculations. The keyword (integral = grid = ultrafine) was used for all calculations. The 3D images of all optimized geometries were generated with CYLview,⁴² and GaussView⁴³ was used to construct all structures prior to optimization and to visualize the output from the Gaussian 09 calculations.

General Information. Materials were obtained from commercial suppliers and were used without further purification unless otherwise specified. All solvents were of technical grade and used without further purification. Unless otherwise stated, all reactions were performed under ambient conditions. Flash column chromatography was performed on neutral Brockmann I grade aluminum oxide. Reactions were monitored by nuclear magnetic resonance (NMR) with a Bruker DPX-300 spectrometer (¹H 300 MHz, ¹³C 75.5 MHz) in CDCl₃. The observed chemical shifts are reported as δ -values (ppm) relative to tetramethylsilane (TMS). Coupling constants (*J*) are recorded in hertz. Multiplicities are reported as follows: s (singlet), d (doublet), t (triplet), q (quartet), m (multiplet), dd (doublet of doublets), dt (doublet of triplets), td (triplet of doublets), br (broad singlet). Mass spectra were obtained on a MSI/Kratos concept IS mass spectrometer. Vinyl ethers were prepared according to literature procedures⁴⁴ and the spectra match accordingly.

General Procedure using H₂O as Proton Source. To a stirred solution of vinyl ether (3.0 mmol) and isocyanide (1.2 mmol) in THF (0.5 mL) were quickly added CSA (4 mol %) and distilled water (3.0 mmol), respectively. The solution was stirred at room temperature

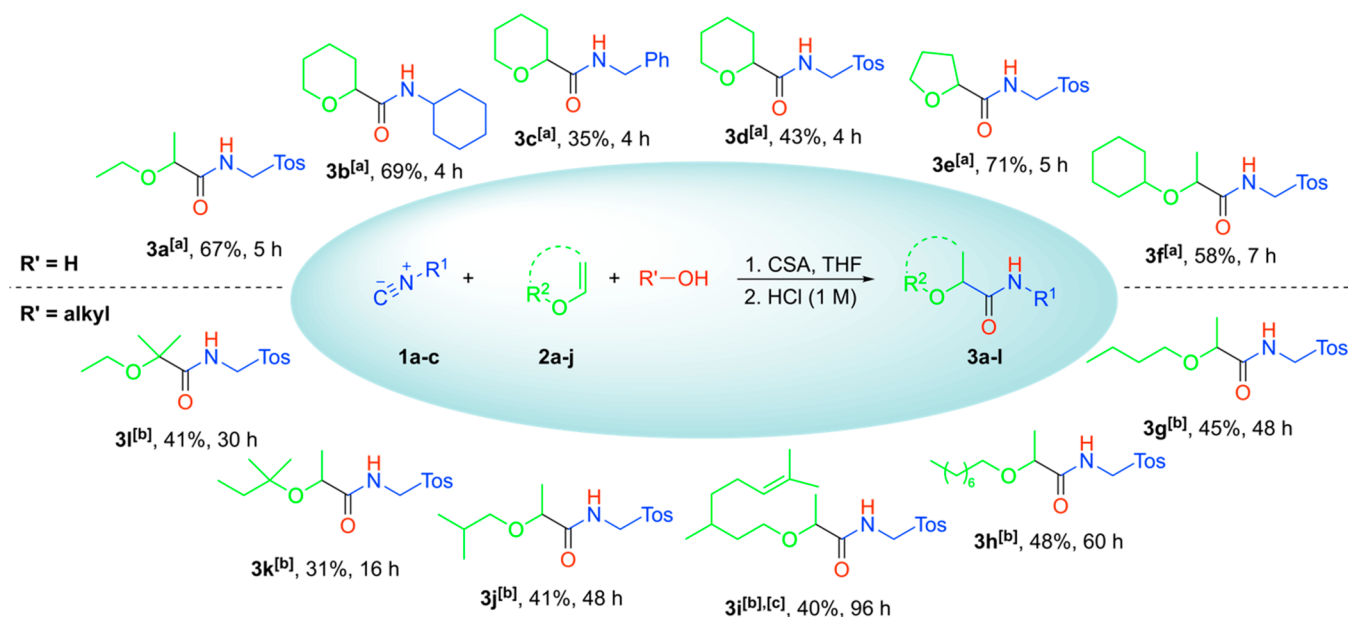
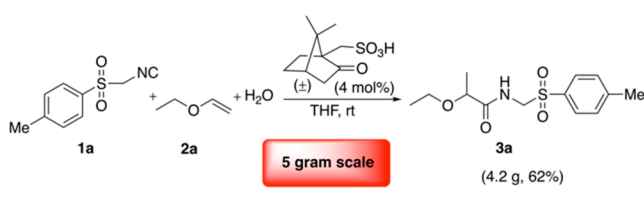


Figure 5. Substrate scope using varying conditions denoted as either “[a]” involving water or as “[b]” involving alcohol; see the Supporting Information for details. [c] indicates the diastereomeric ratio (dr) of compound **3i** is 1:1. The yields provided are reported as isolated yields after flash chromatography.

Scheme 2. Multi-Gram-Scale Reaction



until full consumption of isocyanide was observed via TLC. The reaction was quenched with 1 M HCl, separated with DCM, and concentrated. After removal of solvent, the crude material was subjected to flash column chromatography to furnish the product.

Alternative Procedure using Alcohol as Proton Source. To a stirred solution of vinyl ether (3.0 mmol) and isocyanide (1.2 mmol) in THF (0.5 mL) were quickly added CSA (30 mol %) and alcohol (12.0 mmol), respectively. The solution was stirred at room temperature until full consumption of isocyanide was observed via TLC. The reaction was quenched with 1 M HCl, separated with DCM and concentrated. After removal of solvent, the crude material was subjected to flash column chromatography to furnish the product.

Characterization Data. *2-Ethoxy-N-(tosylmethyl)propanamide (3a)*: (0.230 g, 67%), yellow solid; mp 71–73 °C (hexanes/EtOAc = 3:1); 1H NMR (300 MHz, $CDCl_3$, 25 °C): δ = 1.26–1.32 (m, 6H), 2.45 (s, 3H), 3.41–3.61 (m, 2H), 3.70–3.77 (dd, J = 13.5, 6.6 Hz, 1H), 4.63–4.77 (m, 2H), 7.34–7.37 (d, J = 8.1 Hz, 2H), 7.78–7.81 (d, J = 8.1 Hz, 2H); $^{13}C\{^1H\}$ NMR (75.5 MHz, $CDCl_3$, 25 °C) δ = 15.3, 18.2, 21.7, 59.6, 65.6, 75.9, 128.9, 129.9, 133.8, 145.4, 173.0; HRMS (EI-DFS) m/z $[M + H]^+$ Calcd for $C_{13}H_{19}NO_4S$ 285.1035; Found 285.1027.

N-Cyclohexyltetrahydro-2H-pyran-2-carboxamide (3b):⁴⁵ (0.174 g, 69%), white solid; mp 69–71 °C (hexanes/EtOAc = 3:1); 1H NMR (300 MHz, $CDCl_3$, 25 °C) δ = 1.12–1.28 (m, 4H), 1.32–1.42 (m, 3H), 1.53–1.58 (m, 3H), 1.64 (br, 2H), 1.70–1.76 (dt, J = 12.9, 2.8 Hz, 2H), 1.90–1.93 (m, 3H), 2.13–2.17 (d, J = 13.2 Hz, 1H), 3.45–3.53 (td, J = 10.4, 3.7 Hz, 1H), 3.73–3.79 (m, 2H), 4.03–4.05 (dt, J = 11.0, 1.9 Hz, 1H), 6.45 (br, 1H); $^{13}C\{^1H\}$ NMR (75.5 MHz, $CDCl_3$, 25 °C) δ = 23.2, 24.9, 25.6, 25.7, 29.3, 33.1, 33.1, 47.4, 68.3; HRMS (CI-DFS) m/z $[M + H]^+$ Calcd for $C_{12}H_{22}NO_2$ 212.1651; Found 212.1647.

N-Benzyltetrahydro-2H-pyran-2-carboxamide (3c): (0.092 g, 35%), pink solid; mp 63–65 °C (hexanes/EtOAc = 3:1); 1H NMR (300 MHz, $CDCl_3$, 25 °C) δ = 1.41–1.50 (m, 3H), 1.55–1.58 (m, 3H), 1.92–1.95 (m, 1H), 2.17–2.22 (dd, J = 12.6, 3.0 Hz, 1H), 3.45–3.53 (m, 1H), 3.83–3.87 (dd, J = 11.1, 2.4 Hz, 1H), 4.00–4.05 (dd, J = 10.5, 2.1 Hz, 1H), 4.47–4.49 (d, J = 5.7 Hz, 2H), 6.88 (br, 1H), 7.28–7.38 (m, 5H); $^{13}C\{^1H\}$ NMR (75.5 MHz, $CDCl_3$, 25 °C) δ = 23.2, 25.6, 29.3, 42.8, 68.3, 127.4, 127.8, 128.7, 138.2, 171.9; HRMS (EI-DFS) m/z $[M + H]^+$ Calcd for $C_{13}H_{17}NO_2$ 219.1259; Found 219.1258.

N-(Tosylmethyl)tetrahydro-2H-pyran-2-carboxamide (3d): (0.153 g, 43%), white solid; mp 89–91 °C (hexanes/EtOAc = 1:1); 1H NMR (300 MHz, $CDCl_3$, 25 °C) δ = 1.54 (br, 4H), 1.84–1.88 (d, J = 10.5 Hz, 2H), 2.45 (s, 3H), 3.43–3.51 (m, 1H), 3.64–3.87 (dd, J = 11.7, 2.1 Hz, 1H), 4.05–4.09 (d, J = 12.0 Hz, 1H), 4.58–4.77 (m, 2H), 7.34–7.37 (d, J = 8.1 Hz, 2H), 7.79–7.81 (d, J = 8.4 Hz, 2H); $^{13}C\{^1H\}$ NMR (75.5 MHz, $CDCl_3$, 25 °C) δ = 21.7, 22.9, 25.5, 28.8, 29.7, 59.5, 68.3, 128.9, 129.8, 133.8, 145.8, 171.5; HRMS (EI-DFS) m/z $[M + H]^+$ Calcd for $C_{14}H_{20}NO_4S$ 298.1113; Found 298.1110.

N-(Tosylmethyl)tetrahydro-2H-furan-2-carboxamide (3e): (0.241 g, 71%), white solid; mp 131–133 °C (DCM/EtOAc = 9:1); 1H NMR (300 MHz, $CDCl_3$, 25 °C) δ = 1.73–1.93 (m, 3H), 2.11–2.20 (m, 1H), 2.45 (s, 3H), 3.83–3.99 (m, 2H), 4.19–4.23 (dd, J = 8.3, 4.8 Hz, 1H), 4.53–4.60 (dd, J = 14.0, 6.6 Hz, 1H), 4.76–4.83 (dd, J = 14.0, 7.4 Hz, 1H), 7.34–7.37 (d, J = 8.0 Hz, 2H), 7.44 (br, 1H), 7.77–7.80 (d, J = 8.3 Hz, 2H); $^{13}C\{^1H\}$ NMR (75.5 MHz, $CDCl_3$, 25 °C) δ = 21.7, 25.4, 30.0, 59.6, 69.6, 77.9, 128.9, 129.9, 133.8, 145.5, 172.9; HRMS (EI-DFS) m/z $[M + H]^+$ Calcd for $C_{13}H_{17}NO_4S$ 283.0878; Found 283.0870.

2-(Cyclohexyloxy)-N-(tosylmethyl)propanamide (3f): (0.236 g, 58%), yellow solid; mp 93–95 °C (DCM/EtOAc = 9:1); 1H NMR (300 MHz, $CDCl_3$, 25 °C) δ = 1.17–1.20 (d, J = 6.8 Hz, 3H), 1.23–1.34 (m, 6H), 1.71–1.87 (m, 4H), 2.45 (s, 3H), 3.24–3.30 (m, 1H), 3.81–3.88 (q, J = 6.9 Hz, 1H), 4.62–4.78 (m, 2H), 7.33–7.36 (d, J = 8.1 Hz, 2H), 7.40–7.45 (t, J = 6.6 Hz, 1H), 7.78–7.80 (d, J = 8.4 Hz, 2H); $^{13}C\{^1H\}$ NMR (75.5 MHz, $CDCl_3$, 25 °C) δ = 19.1, 21.7, 23.9, 24.1, 25.50, 32.5, 59.5, 73.3, 128.9, 129.8, 133.7, 145.4, 173.6; HRMS (EI-DFS) m/z $[M + H]^+$ Calcd for $C_{17}H_{25}NO_4S$ 339.1504; Found 339.1499.

2-Butoxy-N-(tosylmethyl)propanamide (3g): (0.169 g, 45%), yellow solid; mp 109–111 °C (DCM/EtOAc = 9:1); 1H NMR

(300 MHz, CDCl₃, 25 °C) δ = 0.95–0.99 (t, J = 7.3 Hz, 3H), 1.18–1.21 (d, J = 6.9 Hz, 3H), 1.27–1.45 (m, 4H), 1.58–1.66 (m, 4H), 2.45 (s, 3H), 3.37–3.52 (m, 2H), 3.68–3.75 (m, 1H), 4.63–4.77 (m, 2H), 7.34–7.37 (d, J = 7.8 Hz, 2H), 7.78–7.81 (d, J = 8.1, 2H); ¹³C{¹H} NMR (75.5 MHz, CDCl₃, 25 °C) δ = 13.8, 18.1, 19.3, 21.7, 29.7, 31.78, 59.5, 70.0, 76.0, 128.9, 129.8, 133.8, 145.4, 173.0; HRMS (EI-DFS) m/z [M + H]⁺ Calcd for C₁₅H₂₃NO₄S 313.1348; Found 313.1339.

2-(Octyloxy)-N-(tosylmethyl)propanamide (3h): (0.213 g, 48%), colorless oil (DCM/EtOAc = 9:1); ¹H NMR (300 MHz, CDCl₃, 25 °C) δ = 0.89–0.94 (m, 3H), 1.18–1.21 (d, J = 6.6 Hz, 3H), 1.28–1.39 (m, 10H), 1.57–1.63 (m, 2H), 2.45 (s, 3H), 3.36–3.53 (m, 2H), 3.68–3.75 (m, 1H), 4.62–4.78 (m, 2H), 7.34–7.37 (d, J = 8.1 Hz, 2H), 7.78–7.81 (d, J = 8.4 Hz, 2H); ¹³C{¹H} NMR (75.5 MHz, CDCl₃, 25 °C) δ = 14.1, 18.1, 21.7, 22.6, 26.1, 29.2, 29.4, 29.7, 31.8, 59.5, 70.4, 76.0, 128.9, 129.8, 133.8, 145.4, 173.0; HRMS (FAB-DFS) m/z [M + Na]⁺ Calcd for C₁₉H₃₁NO₄NaS 392.1866; Found 392.1866.

2-((3,7-Dimethyloct-6-en-1-yl)oxy)-N-(tosylmethyl)propanamide (3i): (0.190 g, 40%), pale white oil (DCM/EtOAc = 9:1); ¹H NMR (300 MHz, CDCl₃, 25 °C) δ = 0.83–0.89 (q, J = 6.6 Hz, 4H), 1.10–1.19 (m, 2H), 1.25–1.51 (m, 5H), 1.60–1.69 (m, 9H), 1.95–2.00 (m, 2H), 2.45 (s, 3H), 3.63–3.69 (m, 1H), 4.04–4.10 (m, 1H), 5.06–5.08 (m, 1H), 7.34–7.36 (d, J = 8.1 Hz, 2H), 7.60–7.62 (d, J = 8.1 Hz, 2H); ¹³C{¹H} NMR (75.5 MHz, CDCl₃, 25 °C) δ = 17.6, 19.2, 21.5, 25.3, 25.3, 25.7, 29.2, 36.6, 36.9, 36.9, 62.8, 62.9, 77.2, 124.5, 125.2, 129.7, 131.3, 141.9, 142.6; LRMS (ESI-ion trap) m/z [M + CH₃]⁺ Calcd for C₂₂H₃₅NO₄S 409.2287; Found 409.21. *Note:* This compound could not be reported using HRMS owing to difficulties in ionization and the absence of peaks strong enough for an accurate high-resolution mass measurement.

2-Isobutoxy-N-(tosylmethyl)propanamide (3j): (0.154 g, 41%), colorless oil (DCM/EtOAc = 9:1); ¹H NMR (300 MHz, CDCl₃, 25 °C) δ = 0.97–0.99 (d, J = 4.5 Hz, 6H), 1.19–1.22 (d, J = 6.6 Hz, 3H), 1.60 (s, 1H), 1.84–1.97 (m, 1H), 3.16–3.30 (m, 2H), 3.68–3.75 (q, J = 6.9, 1H), 4.69–4.72 (dd, J = 6.9, 3.3 Hz), 7.34–7.37 (d, J = 8.1 Hz, 2H); ¹³C{¹H} NMR (75.5 MHz, CDCl₃, 25 °C) δ = 17.9, 19.2, 19.3, 21.7, 28.5, 59.5, 76.2, 128.9, 129.9, 133.8, 145.4, 172.9; HRMS (FAB-DFS) m/z [M + Na]⁺ Calcd for C₁₅H₂₃NO₄NaS 336.1240; Found 336.1256.

2-(tert-Pentyloxy)-N-(tosylmethyl)propanamide (3k): (0.122 g, 31%), white solid; mp 85–87 °C (DCM/EtOAc = 9:1); ¹H NMR (300 MHz, CDCl₃, 25 °C) δ = 0.90–0.95 (t, J = 7.5 Hz, 3H), 1.14 (s, 6H), 1.15–1.17 (d, J = 6.9 Hz, 3H), 1.48–1.57 (m, 2H), 2.45 (s, 3H), 3.90–3.97 (q, J = 6.6 Hz, 1H), 4.69–4.71 (d, J = 6.6 Hz, 2H), 7.34–7.37 (d, J = 8.1 Hz, 2H), 7.42–7.46 (t, J = 6.3 Hz, 1H), 7.79–7.81 (d, J = 8.1 Hz, 2H); ¹³C{¹H} NMR (75.5 MHz, CDCl₃, 25 °C) δ = 8.6, 21.1, 21.7, 25.0, 34.1, 59.6, 76.6, 77.0, 77.2, 77.4, 128.8, 129.8, 134.0, 145.4, 174.5; HRMS (CI-DFS) m/z [M + H]⁺ Calcd for C₁₆H₂₆NO₄S 328.1583; Found 328.1576.

2-Ethoxy-2-methyl-N-(tosylmethyl)propanamide (3l): (0.147 g, 41%), colorless oil. (DCM/EtOAc = 9:1); ¹H NMR (300 MHz, CDCl₃, 25 °C) δ = 1.21 (s, 6H), 1.22–1.27 (t, J = 6.9 Hz, 3H), 2.44 (s, 3H), 3.39–3.46 (q, J = 6.9 Hz, 2H), 4.68–4.71 (d, J = 6.9 Hz, 2H), 7.33–7.36 (d, J = 8.1 Hz, 2H), 7.44–7.49 (t, J = 6.3 Hz, 1H), 7.78–7.81 (d, J = 8.4 Hz, 2H); ¹³C{¹H} NMR (75.5 MHz, CDCl₃, 25 °C) δ = 15.9, 21.7, 23.4, 23.7, 58.7, 59.9, 78.1, 128.9, 129.8, 133.9, 145.3, 175.3; HRMS (FAB-DFS) m/z [M + Na]⁺ Calcd for C₁₄H₂₁NO₄NaS 322.1089; Found 322.1084.

N-(4-Methylbenzenesulfonylmethyl)formamide (4):⁴⁶ (0.02 g, 7%), white solid; mp 106–108 °C (DCM/EtOAc = 9:1); ¹H NMR (300 MHz, CDCl₃, 25 °C) δ = 1.54 (br, 4H), 1.84–1.88 (d, J = 10.5 Hz, 2H), 2.47 (s, 3H); 4.71–4.74 (d, J = 6.9 Hz, 2H), 6.67 (br, 1H), 7.37–7.40 (d, J = 8.1 Hz, 1H), 7.80–7.83 (d, J = 8.1 Hz, 2H), 8.11 (s, 1H); ¹³C{¹H} NMR (75.5 MHz, CDCl₃, 25 °C) δ = 21.8, 58.7, 128.8, 130.1, 133.5, 145.8, 160.0; HRMS (EI-DFS) m/z [M + H]⁺ Calcd for C₉H₁₁NO₃S 213.0460; Found 213.0457.

Representative Procedure for Determining Product Inhibition or Catalyst Deactivation. Three independent reactions were conducted in 4 dram vials. The first reaction, coined as “standard

conditions”, was charged with vinyl ether (**2a** or **2b**) (5.9 M) to which was diluted in 1.0 mL of THF. Next, *p*-toluenesulfonylmethyl isocyanide (**1a**) (2.4 M) was added to the stirring solution. Following this, CSA (4 mol %; 0.095 M) and distilled H₂O (3.9 M) were quickly added, respectively. The next experiment followed the same protocol; however, with a consistent reduction in the initial concentrations of substrates by 0.4 M, i.e., **2a** = 5.5 M, **1a** = 2.0 M, and H₂O = 3.5 M. The third experiment was performed utilizing the conditions from experiment 2 with product added (**3a** or **3b** = 0.9 M). All reactions were allowed to stir for ~2 h. The reaction progress was determined by ¹H NMR (CDCl₃) spectroscopy analyses of aliquots taken periodically. Conversion involved monitoring the disappearance of the signal at 7.88 ppm for **1a** and appearance of the signals ~7.76 ppm for products **3a** or **3b** and 8.03 ppm for side product **4**. *Note:* Signal overlap between the hydroamidated product, e.g., **3a** and side product **4** was observed ~7.76 ppm resulting in constructive interference. This was accounted for when determining product conversion, and thus, product conversion was presented in the absence of inconsistencies.

Representative Procedure for Determining the Order in Catalyst. Using the “standard conditions” data obtained from the experiments involving catalyst deactivation, two additional independent reactions were conducted in 4 dram vials charged with vinyl ether (**2a** or **2b**) (5.9 M) which were diluted in 1.0 mL of THF. Next, *p*-toluenesulfonylmethyl isocyanide (**1a**) (2.4 M) was added to the stirring solutions. Following this, CSA (1, 10, or 20 mol %; 0.024, 0.24, or 0.48 M, respectively) and distilled H₂O (3.9 M) were quickly added, respectively. The reactions were allowed to stir for ~2 h. Reaction progress was determined by ¹H NMR (CDCl₃) spectroscopy analyses of aliquots taken periodically. Conversion involved monitoring the disappearance of the signal at 7.88 ppm for **1a** and appearance of the signals ~7.76 ppm for products **3a** or **3b** and 8.03 ppm for side product **4**.

Representative Procedure for Determining the Reaction Order Dependence of Substrate, e.g., Isocyanide Dependence. Using the “standard conditions” data obtained from the experiments involving catalyst deactivation, two additional independent reactions were conducted in 4 dram vials charged with vinyl ether (**2a** or **2b**) (5.9 M) to which were diluted in 1.0 mL of THF. Next, *p*-toluenesulfonylmethyl isocyanide (**1a**) (1.8- or 1.4 M) was added to the stirring solutions. Following this, CSA (4 mol %; 0.095 M) and distilled H₂O (3.9 M) were quickly added, respectively. The reactions were allowed to stir for ~2 h. Reaction progress was determined by ¹H NMR (CDCl₃) spectroscopy analyses of aliquots taken periodically. Conversion involved monitoring the disappearance of the signal at 7.88 ppm for **1a** and appearance of the signals ~7.76 ppm for products **3a** or **3b** and 8.03 ppm for side product **4**. *Note:* Reaction order dependencies for vinyl ether and H₂O were determined in a similar fashion by using the data from the “standard conditions” reactions followed by additional experiments with varying concentrations of the respective substrate.

Procedure for Determining the Kinetic Solvent Isotope Effect. Two independent reactions were conducted in NMR tubes, maintaining similar concentrations as established in the round-bottom flask. On this front, ethyl vinyl ether (**2a**) (2.1 mmol), *p*-toluenesulfonylmethyl isocyanide (**1a**) (0.84 mmol), CSA (4 mol %), and (D)₂O (2.1 mmol) were quickly added to 0.35 mL of THF in a 4 dram vial. The respective mixture was allowed to sit for 2 min prior to transfer to the NMR tube. Conversion was tracked over a period of ~90 min with data being collected periodically. This involved monitoring the rate of isocyanide consumption. Once the reactions reached ~50% isocyanide consumption, the respective rate constants were estimated from each plot by employing Bruker’s Dynamics Center program. From these rate constants, a normal KSIE (1.7) was observed using the following equation:

$$k_{\text{H}_2\text{O}}/k_{\text{D}_2\text{O}}$$

Procedure for Addition of D₂O to DHP in the Presence of Deuterated CSA. To initiate this study, CSA (0.2 g, 0.86 mmol) was dissolved in 0.78 mL of D₂O (43 mmol) and stirred for 1 h at room temperature in a 4 dram vial. Next, the solution was concentrated *in*

vacuo and the process repeated once more. The deuterium content of the catalyst was verified with HRMS (EI-DFS) measurements: HRMS (EI-DFS) m/z $[M + H]^+$ Calcd for $C_{10}H_{15}DO_4S$ 233.0832; Found 233.0827 and 234.0892.

■ ASSOCIATED CONTENT

Supporting Information

The Supporting Information is available free of charge at <https://pubs.acs.org/doi/10.1021/acs.joc.0c03017>.

Kinetic and experimental methods, computational data, and NMR spectra (PDF)

■ AUTHOR INFORMATION

Corresponding Author

Travis Dudding – Department of Chemistry, Brock University, St. Catharines, ON L2S 3A1, Canada; orcid.org/0000-0002-2239-0818; Email: tdudding@brocku.ca

Authors

Ivor Smajlagic – Department of Chemistry, Brock University, St. Catharines, ON L2S 3A1, Canada

Brenden Carlson – Department of Chemistry, Brock University, St. Catharines, ON L2S 3A1, Canada

Complete contact information is available at:

<https://pubs.acs.org/doi/10.1021/acs.joc.0c03017>

Notes

The authors declare no competing financial interest.

■ ACKNOWLEDGMENTS

T.D. acknowledges financial support from the Natural Science and Engineering Research Council (NSERC) Discovery Grant (2019-04205). I.S. acknowledges QEII-GSST for funding. Computations were carried out using facilities at SHARCNET (Shared Hierarchical Academic Research Computing Network: www.sharcnet.ca) and Compute/Calcul Canada.

■ REFERENCES

(1) Selected examples: (a) Ananthanarayanan, V. S.; Tetreault, S.; Saint-Jean, A. Interaction of Calcium Channel Antagonists with Calcium: Spectroscopic and Modeling Studies on Diltiazem and its Ca^{2+} Complex. *J. Med. Chem.* **1993**, *36*, 1324–1332. (b) Patchett, A. A. Excursions in Drug Discovery. *J. Med. Chem.* **1993**, *36*, 2051–2058. (c) Naito, R.; Yonetoku, Y.; Okamoto, Y.; Toyoshima, A.; Ikeda, K.; Takeuchi, M. Synthesis and Antimuscarinic Properties of Quinuclidin-3-yl 1,2,3,4-Tetrahydroisoquinoline-2-carboxylate Derivatives as Novel Muscarinic Receptor Antagonists. *J. Med. Chem.* **2005**, *48*, 6597–6606. (d) Branch, S. K.; Agranat, I. New Drug[®] Designations for New Therapeutic Entities: New Active Substance, New Chemical Entity, New Biological Entity, New Molecular Entity. *J. Med. Chem.* **2014**, *57*, 8729–8765. (e) Mikami, S.; Sasaki, S.; Asano, Y.; Ujikawa, O.; Fukumoto, S.; Nakashima, K.; Oki, H.; Kamiguchi, N.; Imada, H.; Iwashita, H.; Taniguchi, T. Discovery of an Orally Bioavailable, Brain-Penetrating, *in vivo* Active Phosphodiesterase 2A Inhibitor Lead Series for the Treatment of Cognitive Disorders. *J. Med. Chem.* **2017**, *60*, 7658–7676.

(2) (a) Humphrey, J. M.; Chamberlin, A. R. Chemical Synthesis of Natural Product Peptides: Coupling Methods for the Incorporation of Noncoded Amino Acids into Peptides. *Chem. Rev.* **1997**, *97*, 2243–2266. (b) Bode, J. W. Emerging Methods in Amide- and Peptide-Bond Formation. *Curr. Opin. Drug Discovery Dev.* **2006**, *9*, 765–775. (c) Cupido, T.; Tulla-Puche, J.; Spengler, J.; Albericio, F. The Synthesis of Naturally Occurring Peptides and Their Analogs. *Curr. Opin. Drug Discovery Dev.* **2007**, *10*, 768–783.

(3) Carey, J. S.; Laffan, D.; Thomson, C.; Williams, M. T. Analysis of the Reactions Used for the Preparation of Drug Candidate Molecules. *Org. Biomol. Chem.* **2006**, *4*, 2337–2347.

(4) Pattabiraman, V. R.; Bode, J. W. Rethinking Amide Bond Synthesis. *Nature* **2011**, *480*, 471–479.

(5) (a) Han, S.-Y.; Kim, Y.-A. Recent Development of Peptide Coupling Reagents in Organic Synthesis. *Tetrahedron* **2004**, *60*, 2447–2467. (b) Montalbetti, C. A. G. N.; Falque, V. Amide Bond Formation and Peptide Coupling. *Tetrahedron* **2005**, *61*, 10827–10852. (c) Valeur, E.; Bradley, M. Amide Bond Formation: Beyond the Myth of Coupling Reagents. *Chem. Soc. Rev.* **2009**, *38*, 606–631.

(6) (a) Abdelmoty, I.; Albericio, F.; Carpino, L. A.; Foxman, B. M.; Kates, S. A. Structural Studies of Reagents for Peptide Bond Formation: Crystal and Molecular Structures of HBTU and HATU. *Lett. Pept. Sci.* **1994**, *1*, 57–67. (b) Reszka, P.; Methling, K.; Lalk, M.; Xiao, Z.; Weisz, K.; Bednarski, P. J. Control of Aspartate Epimerization during the Coupling of Caspase Specific Tetrapeptides with Aromatic Amines by using *N*-[[[(dimethylamino)-1*H*-1,2,3-triazolo[4,5-*b*]-pyridin-1-yl]methylene]-*N*-methylmethanaminium hexafluorophosphate *N*-oxide (HATU) as a Coupling Reagent. *Tetrahedron: Asymmetry* **2008**, *19*, 49–59.

(7) (a) Marder, O.; Shvo, Y.; Albericio, F. Fast Conventional Fmoc Solid-Phase Peptide Synthesis with HCTU. *Chim. Oggi.* **2002**, *20*, 37–42. (b) Hood, C. A.; Fuentes, G.; Patel, H.; Page, K.; Menakuru, M.; Park, J. H. Fast Conventional Fmoc Solid-Phase Peptide Synthesis with HCTU. *J. Pept. Sci.* **2008**, *14*, 97–101.

(8) (a) Speicher, A.; Klaus, T.; Eicher, T. *O*-(1-Benzotriazolyl)-*N,N,N',N'*-tetramethyluronium Hexafluorophosphat (HBTU) und *O*-(7-Aza-1-benzotriazolyl)-*N,N,N',N'*-tetramethyluronium Hexafluorophosphat (HATU) - Two Modern Peptide Coupling Reagents. *J. Prakt. Chem./Chem.-Ztg.* **1998**, *340*, 581–583. (b) Sureshbabu, V. V.; Lalithamba, H. S.; Narendra, N.; Hemantha, H. P. New and Simple Synthesis of Acid Azides, Ureas and Carbamates from Carboxylic Acids: Application of Peptide Coupling Agents EDC and HBTU. *Org. Biomol. Chem.* **2010**, *8*, 835–840.

(9) (a) Wehrstedt, K. D.; Wandrey, P. A.; Heitkamp, D. Explosive Properties of 1-hydroxybenzotriazoles. *J. Hazard. Mater.* **2005**, *126*, 1–7. (b) McKnelly, K. J.; Sokol, W.; Nowick, J. S. Anaphylaxis Induced by Peptide Coupling Agents: Lessons Learned from Repeated Exposure to HATU, HBTU, and HCTU. *J. Org. Chem.* **2020**, *85*, 1764–1768.

(10) (a) Liu, Q.; Zhang, H.; Lei, A. Oxidative Carbonylation Reactions: Organometallic Compounds (R-M) or Hydrocarbons (R-H) as Nucleophiles. *Angew. Chem., Int. Ed.* **2011**, *50*, 10788–10799. (b) Prechtel, M. H. G.; Wobser, K.; Theysen, N.; Ben-David, Y.; Milstein, D.; Leitner, W. Direct Coupling of Alcohols to Form Esters and Amides with Evolution of H_2 Using *in situ* Formed Ruthenium Catalysts. *Catal. Sci. Technol.* **2012**, *2*, 2039–2042. (c) Shi, R.; Lu, L.; Zhang, H.; Chen, B.; Sha, Y.; Liu, C.; Lei, A. Palladium/Copper-Catalyzed Oxidative C-H Alkenylation/*N*-Dealkylative Carbonylation of Tertiary Anilines. *Angew. Chem., Int. Ed.* **2013**, *52*, 10582–10585. (d) Ferguson, J.; Zeng, F.; Alwis, N.; Alper, H. Synthesis of 2(1*H*)-Quinolinones via Pd-Catalyzed Oxidative Cyclocarbonylation of 2-Vinylanilines. *Org. Lett.* **2013**, *15*, 1998–2001. (e) Li, W.; Liu, C.; Zhang, H.; Ye, K.; Zhang, G.; Zhang, W.; Duan, Z.; You, S.; Lei, A. Palladium-Catalyzed Oxidative Carbonylation of *N*-Allylamines for the Synthesis of β -Lactams. *Angew. Chem., Int. Ed.* **2014**, *53*, 2443–2446. (f) Li, W.; Duan, Z.; Zhang, X.; Zhang, H.; Wang, M.; Jiang, R.; Zeng, H.; Liu, C.; Lei, A. From Anilines to Isatins: Oxidative Palladium-Catalyzed Double Carbonylation of C-H Bonds. *Angew. Chem., Int. Ed.* **2015**, *54*, 1893–1896.

(11) (a) Tsuji, Y.; Yoshii, S.; Ohsumi, T.; Kondo, T.; Watanabe, Y. Dodecacarbonylruthenium Catalyzed One-to-One Addition of *N*-Substituted Formamide to Olefins. *J. Organomet. Chem.* **1987**, *331*, 379–385. (b) Kobayashi, Y.; Kamisaki, H.; Yanada, K.; Yanada, R.; Takemoto, Y. A Convenient Synthesis of (E)- α -Alkylidene- γ -Lactams and (E)-3-Alkylideneoxindoles by Rhodium-Catalyzed Intramolecular Hydroamidation. *Tetrahedron Lett.* **2005**, *46*, 7549–7552. (c) Masdeu, C.; Gomez, E.; Williams, N. A.; Lavilla, R. Hydro-, Halo- and Seleno-

Carbamoylation of Cyclic Enol Ethers and Dihydropyridines: New Mechanistic Pathways for Passerini and Ugi-Type Multicomponent Reactions. *QSAR Comb. Sci.* **2006**, *25*, 465–473. (d) Nakao, Y.; Idei, H.; Kanyiva, K. S.; Hiyama, T. Hydrocarbamoylation of Unsaturated Bonds by Nickel/Lewis-Acid Catalysis. *J. Am. Chem. Soc.* **2009**, *131*, 5070–5071. (e) Fujihara, T.; Katafuchi, Y.; Iwai, T.; Terao, J.; Tsuji, Y. Palladium-Catalyzed Intermolecular Addition of Formamides to Alkynes. *J. Am. Chem. Soc.* **2010**, *132*, 2094–2098. (f) Miyazaki, Y.; Yamada, Y.; Nakao, Y.; Hiyama, T. Regioselective Hydrocarbamoylation of 1-Alkenes. *Chem. Lett.* **2012**, *41*, 298–300. (g) Li, B.; Park, Y.; Chang, S. Regiodivergent Access to Five- and Six-Membered Benzo-Fused Lactams: Ru-Catalyzed Olefin Hydrocarbamoylation. *J. Am. Chem. Soc.* **2014**, *136*, 1125–1131. (h) Huang, L.; Arndt, M.; Gooßen, K.; Heydt, H.; Gooßen, L. Late Transition Metal-Catalyzed Hydroamination and Hydroamidation. *Chem. Rev.* **2015**, *115*, 2596–2697.

(12) Shen, B.; Makley, D. M.; Johnston, J. N. Umpolung Reactivity in Amide and Peptide Synthesis. *Nature* **2010**, *465*, 1027–1032.

(13) Stephenson, N. A.; Zhu, J.; Gellman, S. H.; Stahl, S. S. Catalytic Transamidation Reactions Compatible with Tertiary Amide Metathesis under Ambient Conditions. *J. Am. Chem. Soc.* **2009**, *131*, 10003–10008.

(14) (a) Shangguan, N.; Katukojvala, S.; Greenberg, R.; Williams, L. J. The Reaction of Thio Acids with Azides: a New Mechanism and New Synthetic Applications. *J. Am. Chem. Soc.* **2003**, *125*, 7754–7755. (b) Li, X.; Danishefsky, S. J. New Chemistry with Old Functional Groups: On the Reaction of Isonitriles with Carboxylic Acids—A Route to Various Amide Types. *J. Am. Chem. Soc.* **2008**, *130*, 5446–5448. (c) Rao, Y.; Li, X.; Danishefsky, S. J. Thio FCMA Intermediates as Strong Acyl Donors: A General Solution to the Formation of Complex Amide Bonds. *J. Am. Chem. Soc.* **2009**, *131*, 12924–12926. (d) Bode, J. W.; Eros, G.; Noda, H. Rapid Ligations with Equimolar Reactants in Water with the Potassium Acyltrifluoroborate (KAT) Amide Formation. *J. Am. Chem. Soc.* **2014**, *136* (15), 5611–5614.

(15) de Figueiredo, R. M.; Suppo, J.-S.; Campagne, J.-M. Nonclassical Routes for Amide Bond Formation. *Chem. Rev.* **2016**, *116*, 12029–12122.

(16) Sabatini, M. T.; Boulton, L. T.; Sneddon, H. F.; Sheppard, T. D. A Green Chemistry Perspective on Catalytic Amide Bond Formation. *Nat. Catal.* **2019**, *2*, 10–17.

(17) For selected reviews, see: (a) Dömling, A. Recent Developments in Isocyanide Based Multicomponent Reactions in Applied Chemistry. *Chem. Rev.* **2006**, *106*, 17–89. (b) Gulevich, A. V.; Zhdanko, A. G.; Orru, R. V. A.; Nenajdenko, V. G. Isocyanacetate Derivatives: Synthesis, Reactivity, and Application. *Chem. Rev.* **2010**, *110*, 5235–5331. (c) Giustiniano, M.; Basso, A.; Mercalli, V.; Massarotti, A.; Novellino, E.; Tron, G. C.; Zhu, J. To Each His Own: Isonitriles for All Flavors. Functionalized Isocyanides as Valuable Tools in Organic Synthesis. *Chem. Soc. Rev.* **2017**, *46*, 1295–1357.

(18) For selected reviews, see: (a) Dömling, A.; Wang, W.; Wang, K. Chemistry and Biology of Multicomponent Reactions. *Chem. Rev.* **2012**, *112*, 3083–3135. (b) Sadjadi, S.; Heravi, M. M.; Nazari, N. Isocyanide-based Multicomponent Reactions in the Synthesis of Heterocycles. *RSC Adv.* **2016**, *6*, 53203–53272. (c) Wang, Q.; Wang, D.-X.; Wang, M.-X.; Zhu, J. Still Unconquered: Enantioselective Passerini and Ugi Multicomponent Reactions. *Acc. Chem. Res.* **2018**, *51*, 1290–1300.

(19) (a) Varadi, A.; Palmer, T. C.; Dardashti, R. N.; Majumdar, S. Isocyanide-Based Multicomponent Reactions for the Synthesis of Heterocycles. *Molecules* **2016**, *21*, 19–40. (b) Shaabani, S.; Shaabani, A.; Kucera, M.; Dusek, M. A One-Pot Synthesis of Oxazepine-Quinazolinone bis-Heterocyclic Scaffolds via Isocyanide-Based Three-Component Reactions. *Front. Chem.* **2019**, *7*, 1–7.

(20) (a) Maeda, S.; Komagawa, S.; Uchiyama, M.; Morokuma, K. Finding Reaction Pathways for Multicomponent Reactions: The Passerini Reaction is a Four-Component Reaction. *Angew. Chem., Int. Ed.* **2011**, *50*, 644–649. (b) Zhang, J.; Lin, S.-X.; Cheng, D.-J.; Liu, X.-Y.; Tan, B. Phosphoric Acid-Catalyzed Asymmetric Classic Passerini Reaction. *J. Am. Chem. Soc.* **2015**, *137*, 14039–14042.

(c) Ramozzi, R.; Morokuma, K. Revisiting the Passerini Reaction Mechanism: Existence of the Nitrilium, Organocatalysis of Its Formation, and Solvent Effect. *J. Org. Chem.* **2015**, *80*, 5652–5657. (d) Saya, J. M.; Berabez, R.; Broersen, P.; Schuringa, I.; Kruijthof, A.; Orru, R. V. A.; Ruijter, E. Hexafluoroisopropanol as the Acid Component in the Passerini Reaction: One-Pot Access to β -Amino Alcohols. *Org. Lett.* **2018**, *20*, 3988–3991.

(21) (a) Chéron, N.; Ramozzi, R.; El Kaïm, L.; Grimaud, L.; Fleurat-Lessard, P. Challenging 50 Years of Established Views on Ugi Reaction: A Theoretical Approach. *J. Org. Chem.* **2012**, *77*, 1361–1366. (b) de Koning, M. C.; Joosen, M. J. A.; Worek, F.; Nachon, F.; van Grol, M.; Klaassen, S. D.; Alkema, D. P. W.; Wille, T.; de Bruijn, H. M. Application of the Ugi Multicomponent Reaction in the Synthesis of Reactivators of Nerve Agent Inhibited Acetylcholinesterase. *J. Med. Chem.* **2017**, *60*, 9376–9392.

(22) (a) Kanno, K.-i.; Ren, S.; Li, Y.; Nakajima, K.; Takahashi, T. Intermolecular Coupling of Alkynes, Isocyanates, and Acyl Chlorides: an Efficient Method for the Synthesis of 5-Hydroxypyrrol-2(SH)-ones. *Tetrahedron Lett.* **2007**, *48*, 9199–9202. (b) Yanai, H.; Oguchi, T.; Taguchi, T. Direct Alkylative Passerini Reaction of Aldehydes, Isocyanides, and Free Aliphatic Alcohols Catalyzed by Indium(III) Triflate. *J. Org. Chem.* **2009**, *74*, 3927–3929. (c) Lyu, L.; Xie, H.; Mu, H.; He, Q.; Bian, Z.; Wang, J. AlCl₃-catalyzed O-Alkylative Passerini Reaction of Isocyanides, Cinnamaldehydes and Various Aliphatic Alcohols for Accessing α -Alkoxy- β,γ -Enamides. *Org. Chem. Front.* **2015**, *2*, 815–818. (d) Caputo, S.; Basso, A.; Moni, L.; Riva, R.; Rocca, V.; Banfi, L. Diastereoselective Ugi Reaction of Chiral 1,3-Aminoalcohols Derived from an Organocatalytic Mannich Reaction. *Beilstein J. Org. Chem.* **2016**, *12*, 139–143. (e) Agyal, A.; Demjen, A.; Weber, E.; Kovacs, A. K.; Wolfing, J.; Puskas, L. G.; Kanizsai, I. Lewis Acid-Catalyzed Diastereoselective Synthesis of Multisubstituted N-Acylaziridine-2-carboxamides from 2H-Azirines via Joulie-Ugi Three-Component Reaction. *J. Org. Chem.* **2018**, *83*, 3570–3581.

(23) For selected examples, see: (a) Denmark, S. E.; Fan, Y. The First Catalytic, Asymmetric α -Additions of Isocyanides. Lewis-Base Catalyzed, Enantioselective Passerini-Type Reactions. *J. Am. Chem. Soc.* **2003**, *125*, 7825–7827. (b) Yue, T.; Wang, M.-X.; Wang, D.-X.; Zhu, J. Alcohols in Isonitrile-Based Multicomponent Reaction: Passerini Reaction of Alcohols in the Presence of O-Iodoxybenzoic Acid. *Angew. Chem., Int. Ed.* **2008**, *47*, 9454–9457. (c) Cioc, R. C.; Estevez, V.; van der Niet, D. J.; VandéVelde, C. M. L.; Turrini, N. G.; Hall, M.; Faber, K.; Ruijter, E.; Orru, R. V. A. Stereoselective Synthesis of Functionalized Bicyclic Scaffolds by Passerini 3-Center-2-Component Reactions of Cyclic Ketoacids. *Eur. J. Org. Chem.* **2017**, *2017*, 1262–1271.

(24) For selected examples, see: (a) Znabet, A.; Ruijter, E.; de Kanter, F. J. J.; Köhler, V.; Helliwell, M.; Turner, N. J.; Orru, R. V. A. Highly Stereoselective Synthesis of Substituted Prolyl Peptides Using a Combination of Biocatalytic Desymmetrization and Multicomponent Reactions. *Angew. Chem., Int. Ed.* **2010**, *49*, 5289–5292. (b) Zhao, W.; Huang, L.; Guan, Y.; Wulff, W. D. Three-component Asymmetric Catalytic Ugi Reaction-Concinnity from Diversity by Substrate Mediated Catalyst Assembly. *Angew. Chem., Int. Ed.* **2014**, *53*, 3436–3441. (c) Zhang, Y.; Ao, Y.-F.; Huang, Z.-T.; Wang, D.-X.; Wang, M.-X.; Zhu, J. Chiral Phosphoric Acid Catalyzed Asymmetric Ugi Reaction by Dynamic Kinetic Resolution of the Primary Multicomponent Adduct. *Angew. Chem., Int. Ed.* **2016**, *55*, 5282–5285. (d) Riva, R. Enantioselective Four-component Ugi reactions. *Science* **2018**, *361*, 1072–1073. (e) Xiong, Q.; Dong, S. X.; Chen, Y. S.; Liu, X. H.; Feng, X. M. Asymmetric Synthesis of Tetrazole and Dihydroisoquinoline Derivatives by Isocyanide-based Multicomponent Reactions. *Nat. Commun.* **2019**, *10*, 2116–2126.

(25) For selected examples, see: (a) Yue, T.; Wang, M.-X.; Wang, D.-X.; Masson, G.; Zhu, J. Brønsted Acid Catalyzed Enantioselective Three-Component Reaction Involving the α -Addition of Isocyanides to Imines. *Angew. Chem., Int. Ed.* **2009**, *48*, 6717–6721. (b) Li, D.; Yang, D.; Wang, L.; Liu, X.; Wang, K.; Wang, J.; Wang, P.; Liu, Y.; Zhu, H.; Wang, R. An Efficient Nickel-Catalyzed Asymmetric

Oxazole-Forming Ugi-Type Reaction for the Synthesis of Chiral Aryl-Substituted THIQ Rings. *Chem. - Eur. J.* **2017**, *23*, 6974–6978.

(26) For selected examples, see: (a) Wang, S.; Wang, M.-X.; Wang, D.-X.; Zhu, J. Asymmetric Lewis Acid Catalyzed Addition of Isocyanides to Aldehydes-Synthesis of 5-Amino-2-(1-hydroxyalkyl)-oxazoles. *Eur. J. Org. Chem.* **2007**, *2007*, 4076–4080. (b) Mihara, H.; Xu, Y. J.; Shepherd, N. E.; Matsunaga, S.; Shibasaki, M. A Heterobimetallic Ga/Yb-Schiff Base Complex for Catalytic Asymmetric α -Addition of Isocyanides to Aldehydes. *J. Am. Chem. Soc.* **2009**, *131*, 8384–8385. (c) Zeng, X.; Ye, K.; Lu, M.; Chua, P.; Tan, B.; Zhong, G. Chiral Brønsted Acid Catalyzed Enantioselective Addition of α -Isocyanacetamides to Aldehydes. *Org. Lett.* **2010**, *12*, 2414–2417.

(27) For selected examples, see: (a) Zhao, X. H.; Liu, X. H.; Mei, H. J.; Guo, J.; Lin, L. L.; Feng, X. M. Asymmetric Dearomatization of Indoles through a Michael/Friedel-Crafts-Type Cascade To Construct Polycyclic Spiroindolines. *Angew. Chem., Int. Ed.* **2015**, *54*, 4032–4035. (b) Luo, W. W.; Yuan, X.; Lin, L. L.; Zhou, P. F.; Liu, X. H.; Feng, X. M. A N,N'-Dioxide/Mg(OTf)₂ Complex Catalyzed Enantioselective α -Addition of Isocyanides to Alkylidene Malonates. *Chem. Sci.* **2016**, *7*, 4736–4740. (c) Zheng, S.-C.; Wang, Q.; Zhu, J. Catalytic Atropenantioselective Heteroannulation between Isocyanacetates and Alkynyl Ketones: Synthesis of Enantioenriched Axially Chiral 3-Arylpyrroles. *Angew. Chem., Int. Ed.* **2019**, *58*, 1494–1498. (d) Li, D.; Wang, L.; Yang, Y.; Zhang, M.; Peng, T.; Yang, D.; Wang, R. Construction of Optically Active 2H- and 3H-Pyrroles by Cyclization and Chirality Maintaining 1,5-Ester Shift Reactions. *Adv. Synth. Catal.* **2019**, *361*, 3744–3750.

(28) (a) Smajlagic, I.; Durán, R.; Pilkington, M.; Dudding, T. Cyclopropenium Enhanced Thiourea Catalysis. *J. Org. Chem.* **2018**, *83*, 13973–13980. (b) Smajlagic, I.; Guest, M.; Durán, R.; Herrera, B.; Dudding, T. Mechanistic Insight toward Understanding the Role of Charge in Thiourea Organocatalysis. *J. Org. Chem.* **2020**, *85*, 585–593.

(29) Nielsen, C. D.-T.; Burés, J. Visual Kinetic Analysis. *Chem. Sci.* **2019**, *10*, 348–353.

(30) Gokel, G.; Ltidke, G.; Ugi, I. In *Isonitrile Chemistry*; Ugi, I., Ed.; Academic Press: New York, 1971; pp 145–199.

(31) (a) Burés, J. Variable Time Normalization Analysis: General Graphical Elucidation of Reaction Orders from Concentration Profiles. *Angew. Chem., Int. Ed.* **2016**, *55*, 16084–16087. (b) Burés, J. A Simple Graphical Method to Determine the Order in Catalyst. *Angew. Chem., Int. Ed.* **2016**, *55*, 2028–2031. (c) Martínez-Carrión, A.; Howlett, M. G.; Alamillo-Ferrer, C.; Clayton, A. D.; Bourne, R. A.; Codina, A.; Vidal-Ferran, A.; Adams, R. W.; Burés, J. Kinetic Treatments for Catalyst Activation and Deactivation Processes based on Variable Time Normalization Analysis. *Angew. Chem., Int. Ed.* **2019**, *58*, 10189–10193.

(32) Van Leusen, D.; Van Leusen, A. M. Synthetic Uses of Tosylmethyl Isocyanide (TosMIC). *Org. React.* **2001**, *57*, 417–666.

(33) Schowen, K. B. J. In *Transition States of Biochemical Processes*; Gandour, R. D., Schowen, R. L., Eds.; Plenum Press: New York, 1978; pp 225–283.

(34) Frisch, M. J.; Trucks, G. W.; Schlegel, H. B.; Scuseria, G. E.; Robb, M. A.; Cheeseman, J. R.; Scalmani, G.; Barone, V.; Mennucci, B.; Petersson, G. A.; Nakatsuji, H.; Caricato, M.; Li, X.; Hratchian, H. P.; Izmaylov, A. F.; Bloino, J.; Zhang, G.; Sonnenberg, J. L.; Hada, M.; Ehara, M.; Toyota, K.; Fukuda, R.; Hasegawa, J.; Ishida, M.; Nakajima, T.; Honda, Y.; Kitao, O.; Nakai, H.; Vreven, T.; Montgomery, J. A., Jr.; Peralta, J. E.; Ogliaro, F.; Bearpark, M.; Heyd, J. J.; Brothers, E.; Kudin, K. N.; Staroverov, V. N.; Kobayashi, R.; Normand, J.; Raghavachari, K.; Rendell, A.; Burant, J. C.; Iyengar, S. S.; Tomasi, J.; Cossi, M.; Rega, N.; Millam, J. M.; Klene, M.; Knox, J. e.; Cross, J. B.; Bakken, V.; Adamo, C.; Jaramillo, J.; Gomperts, R.; Stratmann, R. E.; Yazyev, O.; Austin, A. J.; Cammi, A. R.; Pomelli, C.; Ochterski, J. W.; Martin, R. L.; Morokuma, K.; Zakrzewski, V. G.; Voth, G. A.; Salvador, P.; Dannenberg, J. J.; Dapprich, S.; Daniels, A. D.; Farkas, Ö.; Foresman, J. B.; Ortiz, J. V.; Cioslowski, J.; Fox, D. J. *Gaussian 09*, Revision E.01; Gaussian, Inc., Wallingford, CT, 2009.

(35) Crich, D. En Route to the Transformation of Glycoscience: A Chemist's Perspective on Internal and External Crossroads in Glycochemistry. *J. Am. Chem. Soc.* **2021**, *143*, 17.

(36) Plata, R. E.; Singleton, D. A. A Case Study of the Mechanism of Alcohol-Mediated Morita Baylis-Hillman Reactions. The Importance of Experimental Observations. *J. Am. Chem. Soc.* **2015**, *137*, 3811–3826.

(37) Gensch, T.; Teders, M.; Glorius, F. Approach to Comparing the Functional Group Tolerance of Reactions. *J. Org. Chem.* **2017**, *82*, 9154–9159.

(38) Chai, J.-D.; Head-Gordon, M. Long-Range Corrected Hybrid Density Functionals with Damped Atom-Atom Dispersion Corrections. *Phys. Chem. Chem. Phys.* **2008**, *10*, 6615–6620.

(39) Gonzalez, C.; Schlegel, H. B. Reaction Path Following in Mass-Weighted Internal Coordinates. *J. Phys. Chem.* **1990**, *94*, 5523–5527.

(40) Ukui, K. The Path of Chemical Reactions - The IRC Approach. *Acc. Chem. Res.* **1981**, *14*, 363–368.

(41) Cancès, E.; Mennucci, B.; Tomasi, J. A New Integral Equation Formalism for the Polarizable Continuum Model: Theoretical Background and Applications to Isotropic and Anisotropic Dielectrics. *J. Chem. Phys.* **1997**, *107*, 3032–3041.

(42) Legault, C. Y. *CYLview*, Version 1.0b; Université de Sherbrooke: Quebec, Canada, 2009, <http://www.cylview.org>.

(43) Dennington, R.; Keith, T.; Millam, J. *Gauss View*, Version 5; Semichem, Inc.: Shawnee Mission, 2009.

(44) Werner, G.; Rodygin, K. S.; Kostin, A. A.; Gordeev, E. G.; Kashin, A. S.; Ananikov, V. P. A Solid Acetylene Reagent with Enhanced Reactivity: Fluoride-Mediated Functionalization of Alcohols and Phenols. *Green Chem.* **2017**, *19*, 3032–3041.

(45) Masdeu, C.; Díaz, J. L.; Miguel, M.; Jiménez, O.; Lavilla, R. Straightforward α -Carbamoylation of NADH-like Dihydropyridines and Enol Ethers. *Tetrahedron Lett.* **2004**, *45*, 7907–7909.

(46) Chen, J.; Guo, W.; Wang, Z.; Hu, L.; Chen, F.; Xia, Y. Unexpected Role of *p*-Toluenesulfonylmethyl Isocyanide as a Sulfonylating Agent in Reactions with α -Bromocarbonyl Compounds. *J. Org. Chem.* **2016**, *81*, 5504–5512.